Analyzing Finite Volume

for

Single Phase Flow in Porous Media

Sanjay Kumar Khattri

Department of Mathematics

University of Bergen, Norway

e–mail: sanjay@mi.uib.no

Abstract

Two Point Finite Volume Method (2P-FVM) are extensively used for understanding porous media flow because these methods are fast and simple. In this article, we present numerical analysis of Two Point Finite Volume discretization of pressure equation of a single phase flowing in porous media. We present numerical problems with discontinuous permeability, diagonal permeability together with Neumann and Dirichlet boundary conditions. We analyse effect of the boundary conditions on the conditioning of the discrete systems. We also analyse convergence of the 2P-FVM in various norms (L_2 convergence for pressure and Darcy velocity and L_∞ convergence for pressure) for problems with regularity $\mathbf{H}^{1+\gamma}$, for $\gamma = 0.1, 0.2, \ldots, 0.99$.

Key words: Finite Volume Method; Single Phase Flow; MPFA; TPFA; Anisotropic; Heterogenous; Permeability.

1 Introduction

The article is concerned with analysing convergence of the Two Point Flux Approximation (TPFA) or 2-Point Finite Volume Method (FVM-2P) in a variety of porous medium such as isotropic, anisotropic and heterogenous. We also analyse effect of the boundary conditions on the conditioning of the discrete system. We found that it is easier to solve a system of equations associated with pure Dirichlet boundary condition compared to a discrete system formed on mixed boundary (Neumann and Dirichlet boundary condition).

Two Point Flux Approximation (2-Point Finite Volume Method or 2P-FVM) are widely used for understanding fluid flow in porous media because of the reasons of simplicity and computational efficiency (see [2,3,5,9,11,22,10, and references therein]). For example, Exxon Mobil Corporation's reservoir simulator EM$^{\text{power}^{\text{TM}}}$ [33], Schlumberger's Eclipse [7], the general purpose research simulator at the Stanford University[4], the research simulator at the Norsk Hydro [1], research simulator at the Chevron Texaco [21], research simulators at the University of Bergen [16,17], the well known numerical simulator at the Lawrence Berkeley National Laboratory for capturing dynamics of green house gases in porous medium named TOUGH-2 [23], etc. All of these simulators use 2P-FVM on uniform meshes. Let us consider the following steady

state pressure equation of a single phase flow through porous media [2,9,11,22]

$$-\mathrm{div}\,(\boldsymbol{K}\,\mathrm{grad}\,p) = f \qquad \mathrm{in} \quad \Omega, \qquad (1)$$

$$p(x,y) = p^D \qquad \mathrm{on} \quad \partial\Omega_D, \qquad (2)$$

$$\mathbf{g}(x,y) = -\boldsymbol{K}\,\nabla p \qquad \mathrm{on} \quad \partial\Omega_N. \qquad (3)$$

Here Ω is a polyhedral domain in $\mathbb{R}^d$ ($d = 2,3$), the source function f is assumed to be in $L^2(\Omega)$ and the diagonal tensor coefficient $\boldsymbol{K}(x,y)$ is positive definite and piecewise constant. $\boldsymbol{K}$ is allowed to be discontinuous in space. In porous media flow, the unknown function $p = p(x,y)$ represents the pressure of a single fluid, $\boldsymbol{K}$ is the permeability or hydraulic conductivity of the porous medium Ω and velocity of the fluid phase is given by the Darcy law as $\mathbf{u} = -\boldsymbol{K}\,\mathrm{grad}\,p$ [2,3,9,11,22]. Here $\mathbf{u}$ is the Darcy velocity. In the equations (2) and (3), $\partial\Omega_D$ and $\partial\Omega_N$ represents Dirichlet and Neumann parts of the boundary. On the Dirichlet part pressure is specified and on the Neumann part of the boundary Darcy velocity is specified.

Finite Volume Methods (FMVs) are preferred for discretizing porous media equations because these methods are based on the conservation and continuity of fluxes. FVMs are divided into two classes Multi Point Flux Approximation (MPFA) [7,12–15] and Two Point Flux Approximation (TPFA) [2,3,9,11,22].

TPFA/2P-FVM approximate flux correctly for cartesian tensor grids given the principal directions of the permeability tensor are aligned with the grid direc-

tions [2]. It was found in [5,8] that for full tensor $\boldsymbol{K}$, TPFA results in a consistent flux approximation on streamline-potential grid. Consequently, standard simulators can be applied to arbitrary full tensor field problems provided that a suitable streamline-equipotential grid is generated. Ensuring monotonicity of a discretization scheme is a difficult task [22] and non-monotone scheme can provide unphysical results [2,22]. Apart from being simple and fast one other big advantage of TPFA over MPFA is that TPFA discretization is always monotone [22]. Article [27] presents various domain decomposition methods for Finite Volume Methods. For convergence of TPFA method on uniform and non-uniform meshes, we refer to References [14,13,12,15,29,31, and references therein]. The author like to mention that from the convergence theory of TPFA, we know the convergence behaviour of TPFA under the following conditions

1. Articles [14,13,12] present convergence of Darcy velocity for problems with regularity $\mathbf{H}^{1+\gamma}$ with $\gamma > 0.5$.

2. Articles [31,15] present L_2 convergence of pressure and velocity for problems with sufficiently smooth solution.

3. Article [29] presents convergence for problems with regularity $\mathbf{H}^{1+\gamma}$ with $\gamma > 0.5$.

We present numerical work to understand the convergence of 2P-FVM in different norms for problems with regularity $\mathbf{H}^{1+\gamma}$ with $\gamma > 0.1$. Ten experiments are performed with singularity $\gamma = 0.1, 0.2, \ldots, 0.99$. Our work is a small step

in the direction of the articles [14,13,12,15,29,31] to further understand the convergence behaviour the method.

An outline of the article is as follows. In the Section 2, we present TPFA discretization of the single phase pressure equation. Implementation of Dirichlet and Neumann boundary conditions is also mentioned. Section 3 presents various norms for measuring errors in the scalar pressure and the Darcy velocity. Section 4 presents an extensive numerical analysis of the Two Point Finite Volume discretization of the single phase pressure equation. Finally Section 5 concludes the article.

2 Two Point Finite Volume Discretization

For solving partial differential equations (PDEs) on a domain by numerical methods such as TPFA, the domain is divided into smaller good quality elements (meshing of the domain). These elements are called finite volumes or cells. Integrating equation (1) over one of the finite volumes V in the mesh and using Gauss-Divergence theorem leads to

$$-\int_{\partial V} \boldsymbol{K}\, \nabla p \cdot \hat{\mathbf{n}} = \int_V f, \tag{4}$$

where $\hat{\mathbf{n}}$ is the unit normal on the boundary ∂V and it is pointing away from the center of the cell V. Lets assume that finite volumes V are rectangular

5

or quadrilateral in shape. Boundary of these finite volumes consists of four segments. Then, the above equation can be written as

$$-\sum_{i=1}^{4} \int_{\partial V_i} \boldsymbol{K}\, \nabla p \cdot \hat{\mathbf{n}} = \int_V f, \qquad (5)$$

The term $\int_{\partial V_i} \boldsymbol{K} \nabla p \cdot \hat{\mathbf{n}}$ is referred as the flux through the edge ∂V_i. Lets denote it by $\mathcal{F}_i$. Thus equation (5) can be written as

$$\sum_{i=1}^{4} [-\mathcal{F}_i] = \int_V f. \qquad (6)$$

We call the above equation the conservation of the flux equation. Figure 2 shows the conservation of flux for a finite volume. The degrees of freedom (DOF) for TPFA [2,9,11,10,5] lies at the cell centers. Each finite volume in the mesh give rise to a discrete equation like (6). Collecting all such equations will result in a discrete system $\boldsymbol{A}\, \mathbf{p}_h = \mathbf{b}$. If the flux $\mathcal{F}_i$ across an edge i only depends on the scalar pressure of the two cells sharing this edge then the method of discretization is called Two Point Flux Approximation (TPFA). If the $\mathcal{F}_i$ not only depends on the scalar pressures of the two cells sharing this edge but also on the pressures of the other surrounding cells then the method of discretization is called Multi Point Flux Approximation (MPFA). There are a number of MPFA formulations depending on how the flux expression is formulated [2]. Now lets consider computing $\mathcal{F}_i$ in equation (6).

Figure 1 shows two cells P and E. Let us compute the flux across the common

edge AB of the cells. Let the permeabilities of the cells P and E be

$$\boldsymbol{K}_P = \begin{pmatrix} kx_1 & 0 \\ & \\ 0 & ky_1 \end{pmatrix} \quad \text{and} \quad \boldsymbol{K}_Q = \begin{pmatrix} kx_2 & 0 \\ & \\ 0 & ky_2 \end{pmatrix}.$$

Flux across the edge AB by the TPFA is given as [2]

$$\mathcal{F}_{AB} = \Phi_{AB}\,(p_E - p_P), \tag{7}$$

where Φ_{AB} is referred as the transmissibility of the interface AB and is given as

$$\Phi_{AB} = kx_1\,kx_2\left(\frac{l}{h_1\,h_2}\right)\frac{1}{(kx_1/h_1 + kx_2/h_2)}. \tag{8}$$

Here l is the length of the common edge AB. h_1 is the perpendicular distance from the center of the cell P on the edge AB. Similarly h_2 is defined.

2.1 Implementation of Boundary Conditions

In the case of Finite Volume discretization every finite volume in the mesh will result in discrete equation like (6). Thus for handling boundary cells, boundary conditions are converted into an equivalent flux expression. Flux or Neumann boundary condition can be easily implemented and are more accurate than Dirichlet boundary condition [20].
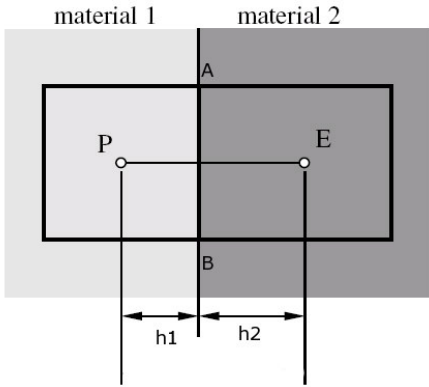
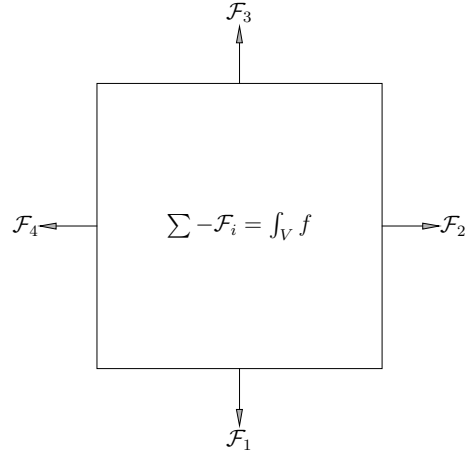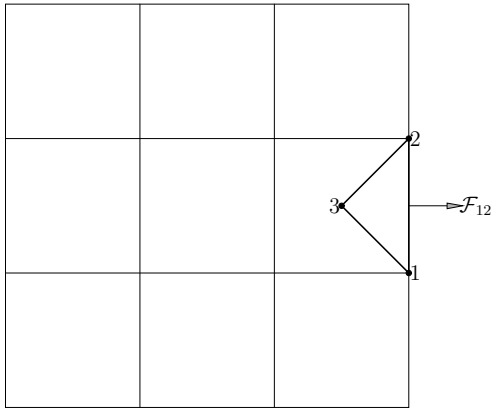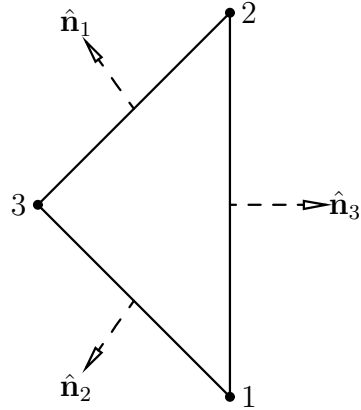Fig. 1. Flux through the interface AB shared by the cells P and E.

Fig. 2. Conservation of flux. Here $\mathcal{F}_i$ with $i = 1 \ldots 4$ are the fluxes through the cell boundaries.

(a) A 3×3 mesh. Pressure is specified at the boundary points 1 and 2. Flux ($\mathcal{F}_{12}$) through the edge 12 is expressed as a linear combination of the pressures at the locations 1, 2 and 3. See the equation (10).

(b) Boundary triangle. Here $\hat{\mathbf{n}}_i$ with $i = 1 \ldots 3$ are the normal vectors on the edges.

Fig. 3. Implementation of the Dirichlet boundary condition.

Since Flux $= -\boldsymbol{K} \nabla p \cdot \hat{\mathbf{n}}$, thus computation of flux across an edge requires computation of pressure gradient. So, lets write an expression for the gradient of the scalar pressure p. Let the pressure at the three vertices of the triangle 3(b) be p_1, p_2 and p_3. Assuming that the pressure is varying linearly inside the triangle. Then the constant gradient of the pressure (∇p) in the triangle

shown in the Figure 3(b) can be expressed as (see [2,20])

$$\nabla p = \frac{-1}{2\,\Omega} \sum_{i=1}^{3} p_i\, \hat{\mathbf{n}}_i.$$ (9)

Here Ω is the area of the triangle and $\hat{\mathbf{n}}_i$ is the normal vector on the edge opposite to the vertex i. The magnitude of the vector $\hat{\mathbf{n}}_i$ is equal to the length of the edge.

2.1.1   Dirichlet Boundary Condition

Figure 3(a) shows a 3×3 mesh. Let the pressure is specified at the boundary points 1 and 2. For applying the conservation principle to the boundary cell 3; i.e., sum of the fluxes through the boundaries of the cell equal to the source inside the cell. We have to compute the flux ($\mathcal{F}_{12}$) through the boundary edge 12. For computing the flux, let us form a boundary triangle 123 as shown in the Figure 3(b). Let the unknown pressure at the center of the boundary cell 3 be p_3. The pressure gradient inside the boundary triangle can be approximated by the expression 9. Thus, the flux through the boundary edge 12 is $F_{12} = -(\boldsymbol{K}\nabla p) \cdot \hat{\mathbf{n}}_3$. Let the outward normal vector on the edge (see the triangle 3(b)) opposite to the vertex i be $\hat{\mathbf{n}}_i = (nx_i, ny_i)^t$. The vector $\hat{\mathbf{n}}_i$ is pointing away from the node i and the magnitude of the vector is equal to the length

of the edge. Let the permeability of the boundary cell 3 be

$$K = \begin{pmatrix} kx & 0 \\ & \\ 0 & ky \end{pmatrix}.$$

Substituting the values of K and ∇p (given by the equation (9)) in the equation $\mathcal{F}_{12} = -(K \nabla p) \cdot \hat{n}_3$ results in

$$\mathcal{F}_{12} = -\frac{1}{2\,\Omega} \left[kx \left(\sum_{i=1}^{3} p_i \, nx_i \right) nx_3 + ky \left(\sum_{i=1}^{3} p_i \, ny_i \right) ny_3 \right]. \qquad (10)$$

Here Ω is the absolute value of the area of the boundary triangle 123.

2.1.2 Flux Boundary Condition

Implementation of Neumann or flux boundary condition is even simpler. Flux across a boundary edge will go on the right hand side vector $\mathbf{b}$ of the discrete system $A\,\mathbf{p}_h = \mathbf{b}$.

3   Discrete Norms

In this section, different norms for measuring error are presented.

3.1 Discrete Norms For Measuring Convergence of Scalar Pressure

Let $\mathbf{p}$ be the exact solution vector and $\mathbf{p}_h$ be the Finite Volume solution vector on a mesh. Let us further assume that p^k denotes the exact pressure at the center of the cell k and p_h^k denotes the discrete pressure by the Finite Volume approximation for the same location. The error in the L_∞ norm is

$$\|\mathbf{p} - \mathbf{p}_h\|_{L_\infty} := \max_{k \in \text{cells}} \left[|p^k(x) - p_h^k(x)| \right], \tag{11}$$

and error in the L_2 norm is

$$\|\mathbf{p} - \mathbf{p}_h\|_{L_2} := \left(\sum_{\text{cells}} \left[p^k(x) - p_h^k(x) \right]^2 \Omega_k \right)^{1/2}. \tag{12}$$

Here Ω_k is the area of the finite volume k in the mesh.

3.2 Discrete Norm For Measuring Convergence of Vector Velocity

Let $\mathbf{u}$ be the exact Darcy velocity through the center of an edge E and $\mathbf{u}_h$ be the discrete Darcy velocity by the Finite Volume method through the center of the same edge E. Let $\hat{\mathbf{n}}$ denotes the normal to the edge E and the magnitude of normal vector $\hat{\mathbf{n}}$ is equal to the length of the edge E. The velocity error $\mathbf{e}$

on a mesh in the $L_2(\Omega)$ norm reads

$$\|\mathbf{u} - \mathbf{u}_h\|_{L_2} := \left(\sum_{\text{cells}} \sum_{\text{edges}} \left[|(\mathbf{u} - \mathbf{u}_h) \cdot \hat{\mathbf{n}}| \right]^2 \right)^{1/2}. \tag{13}$$

It can be seen that the above norm considers each edge twice. It is the L_2 seminorm [6]. For a mesh, we measure errors in norms given by equations (11), (12) and (13).

4   Numerical Examples

For all the numerical examples presented, we use the Conjugate Gradient (CG) linear solver with ILU preconditioner unless mentioned otherwise. Tolerance of the CG solver is 1.0×10^{-10}. We are using $\|\mathbf{p} - \mathbf{p}_h\| = C \, \text{DOF}^{-P/2}$ (or $\|\mathbf{p} - \mathbf{p}_h\| = C \, h^{-P}$) for measuring convergence rate P in different norms as follows

$$P = \frac{\log(\|\mathbf{p} - \mathbf{p}_h\|^n / \|\mathbf{p} - \mathbf{p}_h\|^{n+1})}{\log(\sqrt{\text{DOF}^{n+1}/\text{DOF}^n})}$$

Here h is the size of the smallest finite volume in the mesh. DOF exists for the degrees of freedom and its value is equal to the number of cells or finite volumes in the mesh. For all the numerical experiments, we start with a 2×2 rectangular mesh and successively refined each cell into four cells till 10 level of refinement (mesh dimension $2^n \times 2^n$ and n goes from 1 till 10. Thus, each increment in n will reduce the mesh diameter by half). All numerical examples are performed on a 64 bit machine. For all of the numerical examples presented

the exact solution is given in the analytical form and the solution is enforced inside the domain by the boundary conditions and source term.

4.1 Diagonal Permeability Tensor

Let the exact solution and permeability be

$$p(x, y) = x^3 y^4 + x^2 + \sin(xy) \cos(y), \tag{14}$$

$$\boldsymbol{K} = \begin{pmatrix} (x+1)^2 + y^2 & 0 \\ 0 & (x+1)^2 \end{pmatrix}. \tag{15}$$

The permeability is anisotropic and inhomogeneous in nature. Figure 4 is a surface plot of the exact solution. Figures 5 and 6 present surface plots of the two components of the permeability tensor. The domain is $\Omega = (0, 6) \times (0, 6)$. The solution inside the domain is enforced by source term and Dirichlet boundary condition. This example was also solved in [32] by the Mixed Finite Element Method on multiblock domains

Since the problem is $\mathbf{H}^2$ regular in nature. We expect from the convergence theory of the TPFA [9,31] that both Darcy velocity and pressure should converge like h^{-2} (or DOF^{-1}) in the L_2 norm. Figures 7, 8 and 9 report the outcome of our numerical experiments. It is clear from the Figure 7 that pressure is converging at an optimal rate in L_2 and velocity convergence in the Figure 9
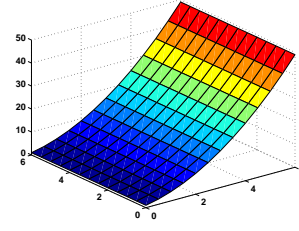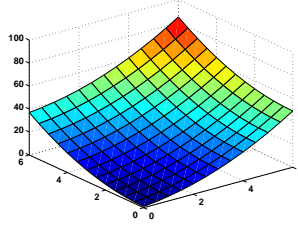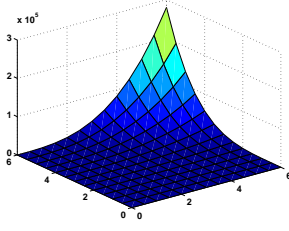
13

Fig. 4. Example 4.1. Exact solution.

Fig. 5. Example 4.1. $\boldsymbol{K}_{11} = (x+1)^2 + y^2$.

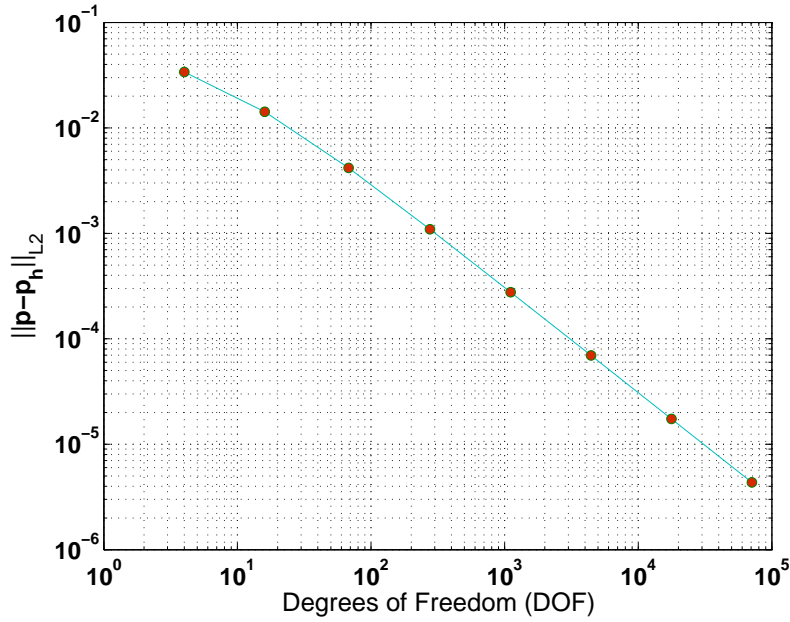Fig. 6. Example 4.1. $\boldsymbol{K}_{22} = (x+1)^2$.

Fig. 7. Example 4.1: L_2 convergence of pressure is $\|\mathbf{p} - \mathbf{p}_h\|_{L_2} \approx C\,\mathrm{DOF}^{-0.999}$. Thus convergence rate $P = 1.9995$.

is less than optimal. Point-wise convergence for pressure as shown in Figure 8

is of the order h^{-2}. We are getting the following convergence behaviour

$$\|\mathbf{p} - \mathbf{p}_h\|_{L_2} \approx C\,\mathrm{DOF}^{-1.99/2}, \quad \|\mathbf{p} - \mathbf{p}_h\|_{L_\infty} \approx C\,DOF^{-1.98/2} \quad \text{and}$$

$$\|\mathbf{u} - \mathbf{u}_h\|_{L_2} \approx C\,\mathrm{DOF}^{-1.49/2}. \tag{16}$$

Thus pressure in the L_2 and L_∞ norms is super-convergent. It can be seen

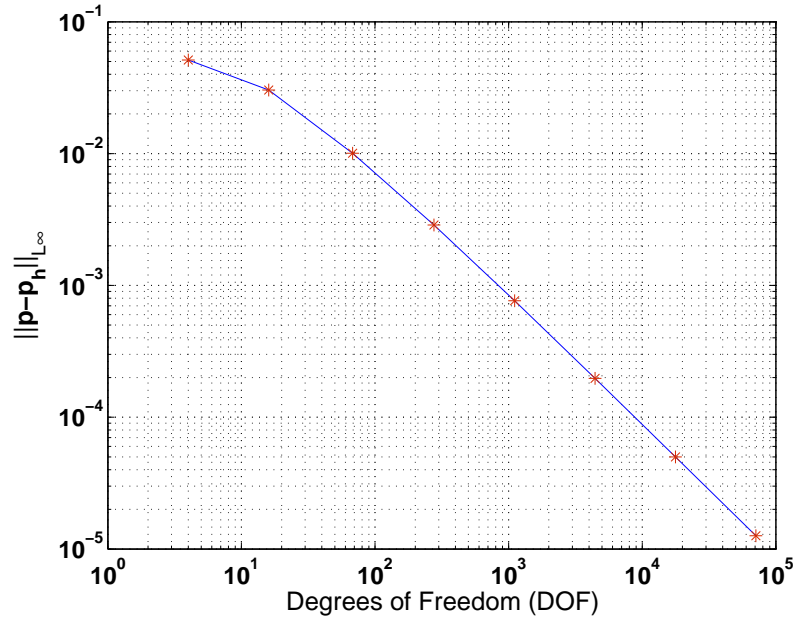that the Darcy velocity is not converging with an expected rate.

14

Fig. 8. Example 4.1: L_∞ convergence of pressure is $\|\mathbf{p} - \mathbf{p}_h\|_{L_\infty} \approx C \, \mathrm{DOF}^{-0.994}$. Convergence rate $P = 1.9888$.
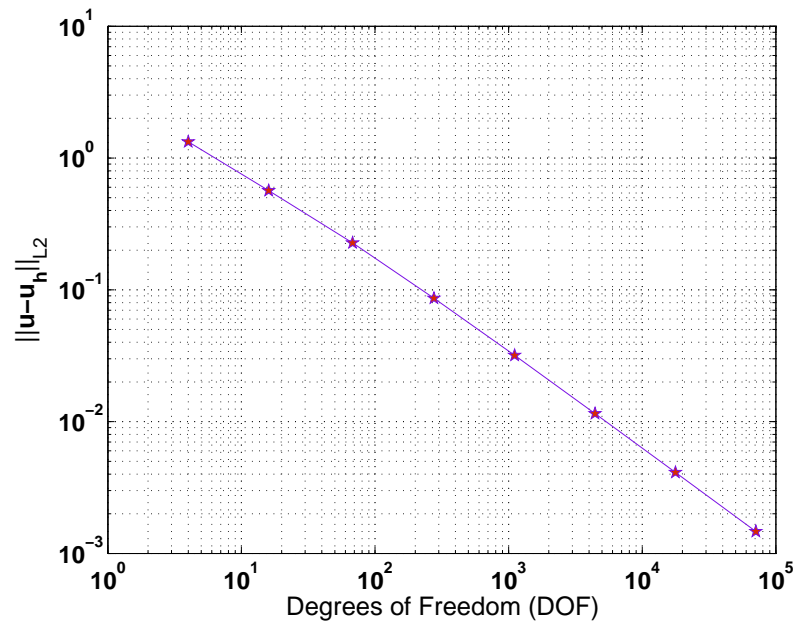

Fig. 9. Example 4.1: L_2 convergence of Darcy velocity is $\|\mathbf{u} - \mathbf{u}_h\|_{L_2} \approx C$ $\mathrm{DOF}^{-0.745}$. Convergence rate $P = 1.4899$.

4.2 Homogenous medium with $\boldsymbol{K} = \boldsymbol{I}$

In the previous example, we are not getting an optimal convergence for the velocity. So, we perform experiment by assuming isotropic and homogenous

medium. Let the permeability be identity tensor; i.e., $\boldsymbol{K} = \boldsymbol{I}$. Let the exact pressure is given by the bubble function; i.e., $p(x, y) = x\,(x - 1)\,y\,(y - 1)$ is the exact solution. The domain is $\Omega = (0, 1) \times (0, 1)$. We enforce the solution inside the domain by the Dirichlet boundary condition and source term.

We are observing the following super-convergence behaviour

$$\|\mathbf{p} - \mathbf{p}_h\|_{L_2} \approx C\,\mathrm{DOF}^{-2.0000/2}, \quad \|\mathbf{p} - \mathbf{p}_h\|_{L_\infty} \approx C\,\mathrm{DOF}^{-2.9887/2} \quad \text{and}$$

$$\|\mathbf{u} - \mathbf{u}_h\|_{L_2} \approx C\,\mathrm{DOF}^{-1.9999/2}. \tag{17}$$

Our final mesh was containing 262144 cells ($2^9 \times 2^9$). We are getting optimal results in all norms (super convergent in all norms).

It can be seen from the above two numerical experiments. For $\mathbf{H}^2$ regular problem, the TPFA discretization is superconvergent in isotropic and homogenous medium. But if the medium is inhomogeneous and anisotropic then the convergence of the Darcy velocity can deteriorate.

4.3 Capturing Singular Solutions by the 2P-FVM

Examples presented are of interest for simulating fluid flow in heterogenous porous medium [3,9,11]. We are solving the single phase pressure equation (1) in the domain $\Omega = (-1, 1) \times (-1, 1)$. The domain is shown in the Figure 10. The domain is divided into four sub-domains according to the permeability $\boldsymbol{K}$

16

(see the Figure 10). The medium properties K is a positive constant in each of the sub-domain and is discontinuous across the surfaces of sub-domains. Let the permeability in the sub-domain Ω_i be K_i. Let us further assume that $K_1 = K_3 = R\,I$ and $K_2 = K_4 = I$. K_1, K_2, K_3 and K_4 refers to the permeability in the subdomains Ω_1, Ω_2, Ω_3 and Ω_4. The parameter R is defined below by the relation (20) and is mentioned in the Table 1. Let the exact solution in the polar form be [19]

$$p(r,\theta) = r^\gamma\,\eta(\theta), \tag{18}$$

where the parameter γ denotes the singularity in the solution [19] and it depends on the permeability distribution in the domain. Figures 11(a) and 11(b) present the permeability distribution for the singularity parameters $\gamma = 0.1$ and $\gamma = 0.5$ respectively. (r,θ) are the polar coordinates of a given point in the domain Ω and $\eta(\theta)$ is given as

$$\eta(\theta) = \begin{cases} \cos((\pi/2 - \sigma)\gamma)\,\cos((\theta - \pi/2 + \rho)\gamma), & 0 \le \theta \le \pi/2, \\[2mm] \cos(\rho\gamma)\,\cos((\theta - \pi + \sigma)\gamma), & \pi/2 \le \theta \le \pi, \\[2mm] \cos(\sigma\gamma)\,\cos((\theta - \pi - \rho)\gamma), & \pi \le \theta < 3\pi/2, \\[2mm] \cos((\pi/2 - \rho)\gamma)\,\cos((\theta - 3\pi/2 - \sigma)\gamma), & 3\pi/2 \le \theta \le 2\pi, \end{cases} \tag{19}$$

17

The parameters γ, ρ and σ satisfy the following nonlinear relations

$$
\begin{cases}
R = -\tan((\pi - \sigma)\gamma)\,\cot(\rho\,\gamma), \\[2ex]
1/R = -\tan(\rho\,\gamma)\,\cot(\sigma\,\gamma), \\[2ex]
R = -\tan(\sigma\,\gamma)\,\cot((\pi/2 - \rho)\,\gamma), \\[2ex]
0 < \gamma < 2, \\[2ex]
\max\{0, \pi\,\gamma - \pi\} < 2\,\gamma\,\rho < \min\{\pi\,\gamma, \pi\}, \\[2ex]
\max\{0, \pi - \pi\,\gamma\} < -2\,\gamma\,\rho < \min\{\pi, 2\,\pi - \pi\,\gamma\}.
\end{cases}
\tag{20}
$$

The constrained nonlinear equations (20) can be solved for the parameters R, σ and ρ by the Newton's iteration algorithm for different degrees of singularity γ. The authors wrote a Newton's iterative algorithm in the C^{++} language for solving constrained non-linear equations (20). Table 1 reports an outcome of our program for various degree of singularity (γ). Since the problems with discontinuous medium properties are of practical applications such as fluid flow in heterogenous porous medium, heat conduction in composite materials, etc. The data presented in the Table 1 can be a good source of analytical solutions for testing and validating softwares.

The analytical solution $p(r, \theta)$ satisfies the usual interface conditions; i.e., p and $\boldsymbol{K}\frac{\partial p}{\partial n}$ are continuous across the interfaces. It can be shown that solution
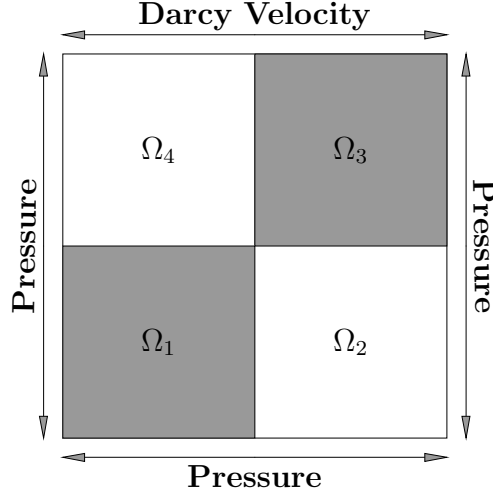
Fig. 10. Example 4.3. Domain is divided into four sub-domains Ω_i, $i = 1 \ldots 4$. Permeability in the sub-domain Ω_i is $\boldsymbol{K}_i$. We are assuming, $\boldsymbol{K}_1 = \boldsymbol{K}_3 = R\,\boldsymbol{I}$ and $\boldsymbol{K}_2 = \boldsymbol{K}_4 = \boldsymbol{I}$. Top edge is on the Neumann boundary condition and rest of the boundary is of Dirichlet type.

p barely belongs in the fractional Sobolev space $\mathbf{H}^{1+\kappa}(\Omega)$ with $\kappa < \gamma$ [28,9]. A surface plot of the exact solution (18) for the singularity $\gamma = 0.1$ is given in the Figure 12(a). For the singularity parameters $\gamma = 0.1$ and $\gamma = 0.5$ the permeability distribution is shown in the Figures 11(a) and 11(b) respectively.

Articles [25,26] (Discontinuous Galerkin Method) and [11] (Finite Volume Method) also report some results for discontinuous permeability. They assumed the boundary was of Dirichlet type, for variety we specified Darcy velocity $\mathbf{u}$ on the top edge and on the rest of the boundary pressure p is specified. In the article [11], only L_2 convergence results are reported. Apart from L_2 convergence, we are also reporting point-wise convergence. The convergence order of the Discontinuous Galerkin for pressure in the L_2 norm is $h^{2\gamma}$ (DOF$^{2\gamma/2}$) [26]. Figures 12(a), 12(b), 13, 14, 15, 16, 17 and 18 report outcome

19

of our numerical experiments.

Figure 12(a) is a surface plot of the exact solution for the singularity parameter $\gamma = 0.1$. Solution shows singular behaviour at the origin. Figure 12(b) presents a surface plot of the error on a 64×64 mesh. It can be seen that the error is maximum at the singularity.

The Figure 13 reports the L_2 convergence of pressure for various degrees of singularity. It can be seen that the convergence rate depends on the regularity (singularity) of the problem. The Figure 14 is a plot of L_2 convergence rate of pressure vs the singularity of the solution. For $\gamma \geq 0.2$, the pressure in the L_2 norm is converging with a rate approximately equal to $2 \times \gamma$ as follows

$$\|\mathbf{p} - \mathbf{p}_h\|_{L_2} \approx C\,\mathrm{DOF}^{-\gamma} \quad \text{or} \quad \|\mathbf{p} - \mathbf{p}_h\|_{L_2} \approx C\,h^{-2\gamma}.$$

It can be seen in the Figure 14 that a high degree of singularity ($0.1 \leq \gamma \leq 0.2$) can retard an expected convergence behaviour ($h^{2\gamma}$). Or, a high degree of singularity requires a high degree of refinement for attaining an asymptotic convergence behaviour. A similar observation is made in the article [11]. For the singularity $\gamma = 0.1269$, the following behaviour is observed in [11]: $\|\mathbf{p} - \mathbf{p}_h\|_{L_2} \approx C\,h^{-1.8\gamma}$.

The Figure 15 is reporting L_∞ convergence of pressure for various degrees of singularity parameter γ. The Figure 16 is plotting the point-wise convergence rate of the TPFA discretization method against the singularity of the underly-

ing solution. The point-wise convergence is dependent on the regularity of the solution and the convergence rate is approximately equal to the singularity of the solution. For the singularity $\gamma = 0.1$, it is interesting to note that the TPFA method does not converge pointwise for more than one million degrees of freedom. For the singularity $\gamma > 0.2$, the pointwise convergence behaviour of the method is

$$\|\mathbf{p} - \mathbf{p}_h\|_{L_\infty} \approx C\,\mathrm{DOF}^{-\gamma/2} \quad \text{or} \quad \|\mathbf{p} - \mathbf{p}_h\|_{L_\infty} \approx C\,h^{-\gamma}.$$

Again an extreme singularity can retard the point-wise convergence of the method. Or, the method need more than 1,000,000 degrees of freedom for attaining an asymptotic convergence rate (DOF^γ). See the Figure 16.

Convergence of the Darcy velocity is reported in the Figure 17. Figure 18 reports the convergence of the Darcy velocity against the singularity of the solution. Again, the convergence of the TPFA discretization is dependent on the regularity of the solution. It is interesting to see how the convergence rate of the method is dependent on the singularity in the solution. For the singularity parameter $\gamma \geq 0.7$, we see that Darcy velocity is converging with a rate approximately equal to 0.50. For $\gamma \geq 0.7$, we are getting the following convergence behaviour

$$\|\mathbf{u} - \mathbf{u}_h\|_{L_2} \approx C\,\mathrm{DOF}^{-0.5/2} \quad \text{or} \quad \|\mathbf{u} - \mathbf{u}_h\|_{L_2} \approx C\,h^{-0.5}.$$

21
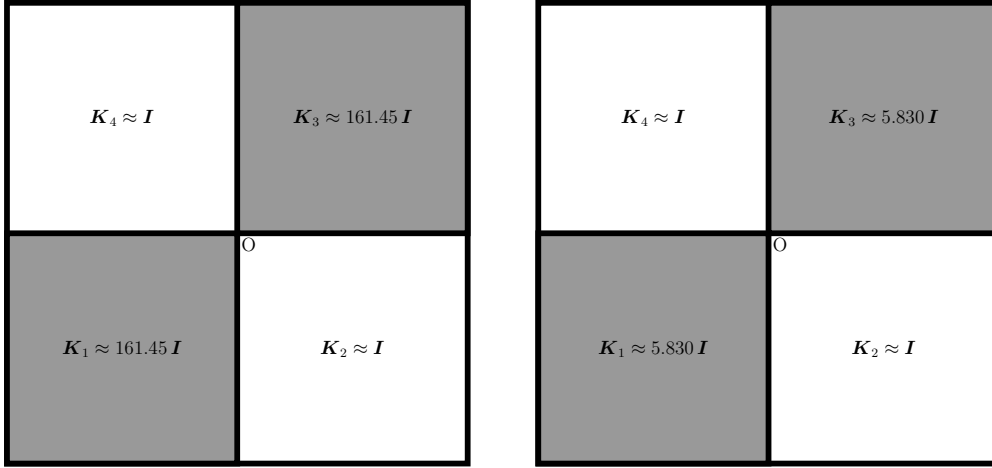
(a) Permeability distribution in $\Omega = (-1,1) \times (-1,1)$ for $\gamma = 0.1$.

(b) Permeability distribution in $\Omega = (-1,1) \times (-1,1)$ for $\gamma = 0.5$.

Fig. 11. Permeability distribution for the singularities $\gamma = 0.1$ and $\gamma = 0.5$. The solution is singular at O=(0,0).

It can be seen in the Figure 18 that for the singularity $\gamma \in [0.2, 0.4]$, roughly the Darcy velocity converges with a rate equal to the singularity of the problem.

The author want to mention a convergence result from the articles [12–14]. The articles [12–14] present convergence analysis of the TPFA and MPFA methods on the locally refined meshes. It is proved in [12] that on the locally refined meshes the TPFA method for problems with regularity $\mathbf{H}^{1+\gamma}$ ($\gamma > 0.5$) converges as $\|\mathbf{u} - \mathbf{u}\|_{L_2} \approx C\,h^{-0.5}$. Thus on the uniform meshes, we can not expect a better convergence.

Table 1
Values of different constants in the equation (19) for different degree of singularity.

γ	R	σ	ρ
0.99	1.031915948135783563	-0.80126479285848151157	0.78539816349999991285
0.95	1.170280531028680322	-0.86807165417883869196	0.78539816349999991285
0.90	1.3708887059534995423	-0.95993108849432950969	0.78539816350000002387
0.85	1.6090769075744693062	-1.0625975150822313253	0.78539816350000002387
0.80	1.8944271903462372997	-1.17809724499362083957	0.78539816349999991285
0.75	2.239828808097679147	-1.3089969388931954608	0.78539816350000002387
0.70	2.6629399279268919365	-1.4585965890641381382	0.78539816349999991285
0.65	3.1884690845675693893	-1.6312115700306100141	0.78539816349999991285
0.60	3.8518399951473525356	-1.8325957144914943875	0.78539816350000002387
0.55	4.7052884457890540304	-2.0705951579452666067	0.78539816349999991285
0.50	5.8284271230555964038	-2.3561944900897935362	0.78539816350000002387
0.45	7.3474532431843240232	-2.7052603404886590432	0.78539816350000002387
0.40	9.4721359523553907422	-3.1415926534872418152	0.78539816349999991285
0.35	12.572219259912507994	-3.7025913416282763002	0.78539816349999991285
0.30	17.349722170012338296	-4.4505895924829887988	0.78539816350000002387
0.25	25.274142362315203059	-5.4977871436795870963	0.78539816350000002387
0.20	39.863458178477991112	-7.0685834704744827661	0.78539816349999991285
0.15	71.384880111309840345	-9.6865773484659776216	0.78539816350000002387
0.10	161.44763875525333674	-14.922565104448967332	0.78539816349999991285
0.05	647.78901130850420031	-30.630528372397932912	0.78539816350000002387
0.02	4052.1806944184704662	-77.7544181762448261	0.78539816350000002387
0.01	16210.722715986315961	-156.29423451598964334	0.78539816349999991285

4.4   Boundary Conditions and the Conjugate Gradient (which meshes are

better conditioned)

In this numerical example, we analyse effect of the boundary conditions on

the conditioning of the discrete systems and the performance of the Conjugate
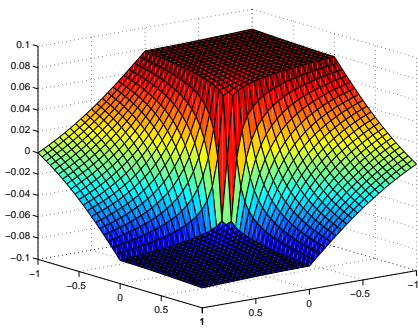
(a) Exact solution given by the equation (18) for $\gamma = 0.1$.
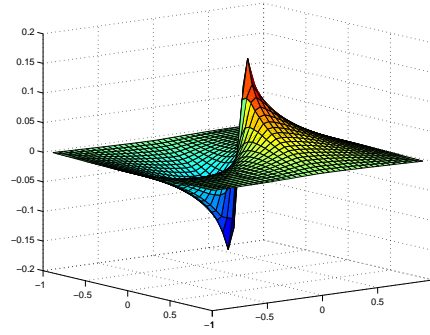
(b) Surface plot of $(p - p_h)/\|p\|_{L_\infty}$ for $\gamma = 0.1$.

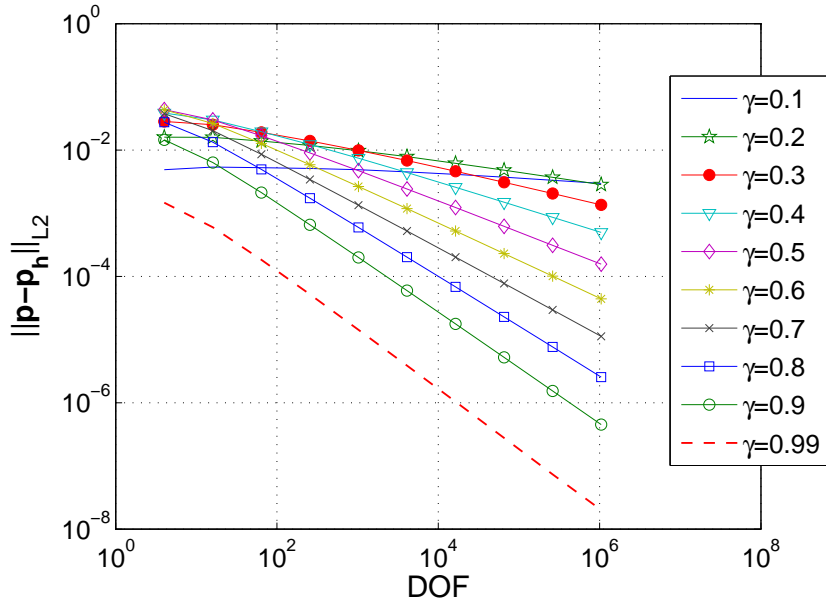Fig. 12. Surface plot of the exact solution and error for the singularity $\gamma = 0.1$.

Fig. 13. Example (4.3): L_2 convergence of scalar pressure for different degree of singularity parameter γ. $\|\mathbf{p} - \mathbf{p}_h\|_{L_2} \approx C \, \mathrm{DOF}^{-\gamma}$. $P \approx 2 \times \gamma$.

Gradient (CG) solver. For the singularity parameter $\gamma = 0.1$, we performed two experiments. In the first experiment, the Darcy velocity is specified on the top edge (Neumann boundary) and pressure is specified on the rest of the boundary (Dirichlet boundary). It is a problem with mixed boundary. In the second experiment, pressure is specified on the whole boundary (Dirichlet
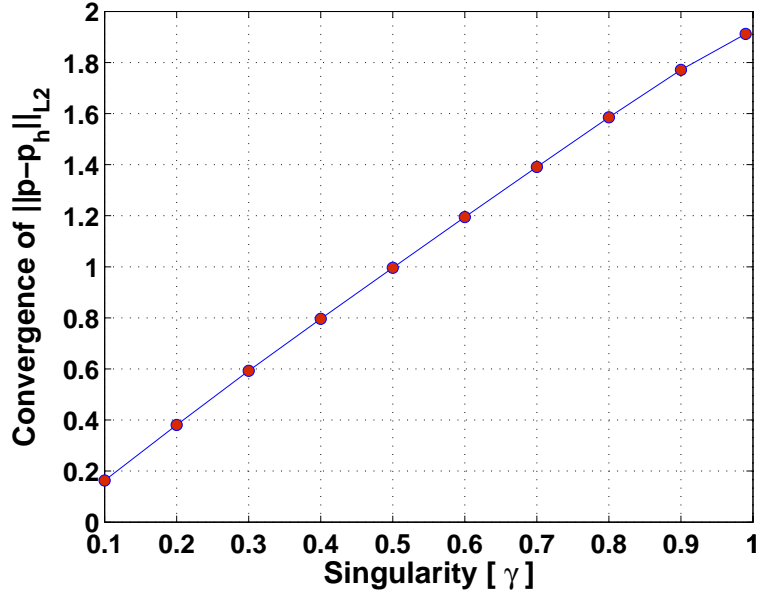
Fig. 14. Example (4.3): Order of L_2 convergence of pressure. $\|\mathbf{p} - \mathbf{p}_h\|_{L_2} \approx C$ $\mathrm{DOF}^{-\gamma}$. Convergence rate $P \approx 2 \times \gamma$.
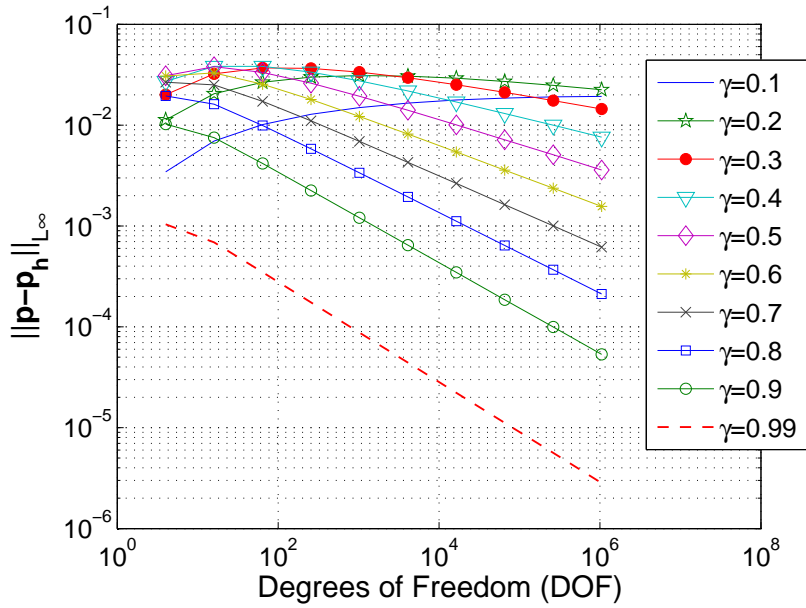

Fig. 15. Example (4.3): Point-wise convergence of pressure for different degree of singularity. $\|\mathbf{p} - \mathbf{p}_h\|_{L_\infty} \approx C\,\mathrm{DOF}^{-\gamma/2}$. Convergence rate $P \approx \gamma$.

boundary). It is a problem with pure Dirichlet boundary. See the Figure 11(a) for the distribution of the permeability field. The exact solution is given by the equation (18).
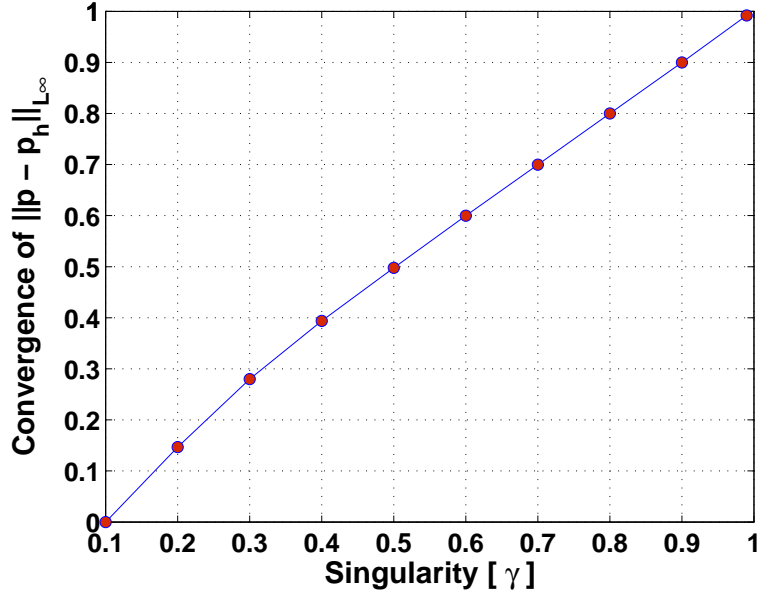
Fig. 16. Example (4.3): Order of L_∞ convergence of pressure. $\|\mathbf{p} - \mathbf{p_h}\|_{L_\infty} \approx C\ \mathrm{DOF}^{-\gamma/2}$. $P \approx \gamma$. We did not see any convergence in L_∞ for $\gamma = 0.1$ till $1.04858 \times 10^{+06}$ DOF. For $\gamma \geq 0.3$, point-wise convergence of the pressure is approximately equal to the singularity of the problem.
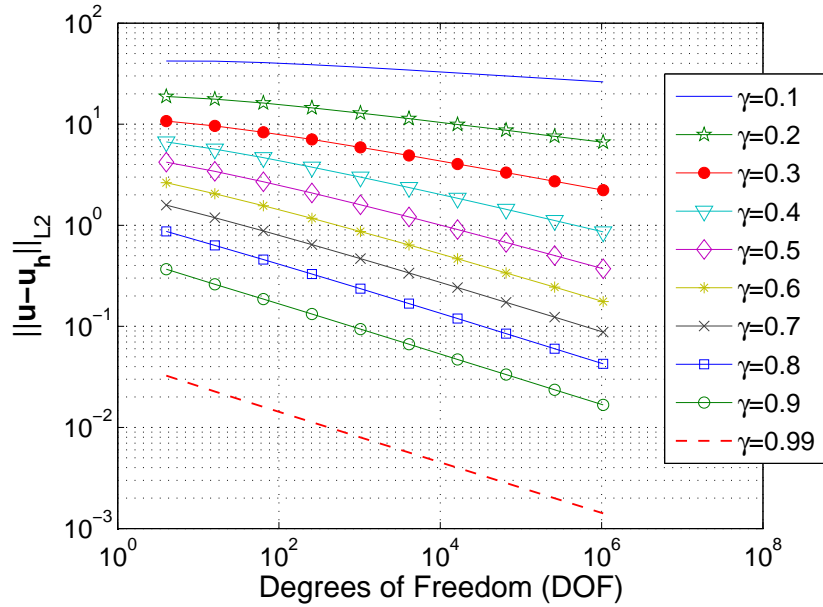

Fig. 17. Example (4.3): Convergence of Darcy Flux for different degree of singularity.
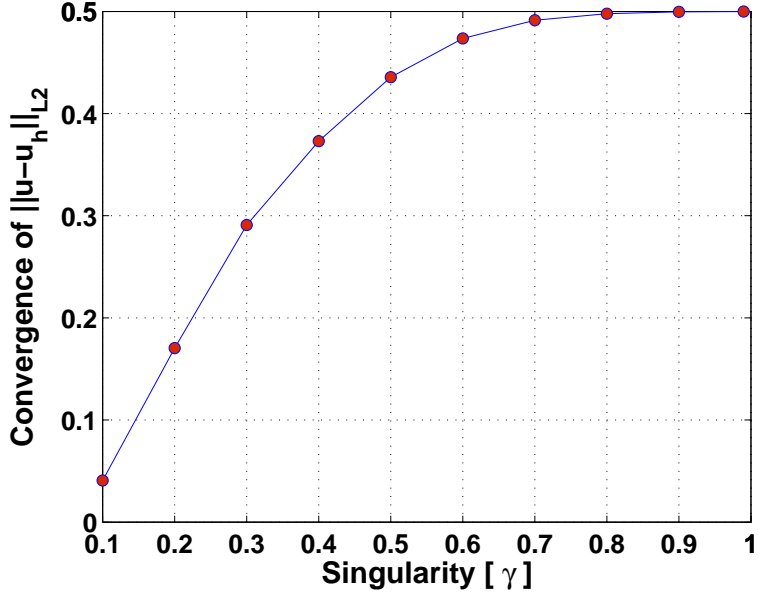
Fig. 18. Example (4.3): Order of L_2 convergence of Darcy Flux. $\|\mathbf{u} - \mathbf{u_h}\|_{L_2} \approx \, ?$.

Figures 19 and 20 are the outcome of our experiments. Before analysing these results, let us first see how the condition number of a matrix and CG-iterations are related. Let $\boldsymbol{A}$ be a symmetric positive definite matrix (SPD) with a condition number $k(= \|\boldsymbol{A}\|_2 \, \|\boldsymbol{A}^{-1}\|_2)$. A well known bound relating the error of the CG iterates (in the matrix norm) with the CG iterations is given as (see [30, chap. 5])

$$\|\mathbf{x}_i - \mathbf{x}\|_{\boldsymbol{A}} \le 2.0 \left(\frac{\sqrt{k} - 1}{\sqrt{k} + 1} \right)^i \|\mathbf{x}_0 - \mathbf{x}\|_{\boldsymbol{A}}, \qquad (21)$$

here $\mathbf{x}_i$ is the solution vector after i Conjugate Gradient iterations. Thus each CG iterate reduces error approximately by $\left[(\sqrt{k} - 1)/(\sqrt{k} + 1) \right]$. Let there

27

be an error reduction of ϵ after n iterations. Thus we can write

$$\left(\frac{1 - \frac{1}{\sqrt{k}}}{1 + \frac{1}{\sqrt{k}}} \right)^n \approx \left(1 - \frac{2.0}{\sqrt{k}} \right)^n \approx e^{-\left(\frac{2.0\, n}{\sqrt{k}} \right)} \approx \epsilon, \tag{22}$$

Thus number of CG iterations needed for reducing error by ϵ are

$$n \approx -\frac{\log \epsilon}{2.0} \sqrt{k}. \tag{23}$$

Let there be two systems $\boldsymbol{A}_{\mathrm{N}} \mathbf{x} = \mathbf{b}_{\mathrm{N}}$ and $\boldsymbol{A}_{\mathrm{D}} \mathbf{x} = \mathbf{b}_{\mathrm{D}}$ with same solution vector $\mathbf{x}$. Let us further assume that the condition numbers of $\boldsymbol{A}_{\mathrm{D}}$ and $\boldsymbol{A}_{\mathrm{N}}$ be k_{D} and k_{N} respectively. Thus from the above relation, number of CG iterations n_{D} and n_{N} required by the systems $\boldsymbol{A}_{\mathrm{D}} \mathbf{x} = \mathbf{b}_{\mathrm{D}}$ and $\boldsymbol{A}_{\mathrm{N}} \mathbf{x} = \mathbf{b}_{\mathrm{N}}$ are related as

$$\frac{n_{\mathrm{D}}}{n_{\mathrm{N}}} \approx \left(\frac{k_{\mathrm{D}}}{k_{\mathrm{N}}} \right)^{1/2}. \tag{24}$$

The Figure 19 is comparing number of preconditioned CG (ILU preconditioner) iterations required for these two problems. It can be seen in this figure that CG is taking about 1.5 times more iterations for the mixed problem than for the Dirichlet problem. Figure 20 is presenting a plot of the number of CG iterations without any preconditioner vs the degrees of freedom for these two problems. It can be notice in this figure that for the mixed boundary conditions CG requires almost twice as many iterations as for the problem with pure Dirichlet boundary. From the relation (24), we conclude that the con-
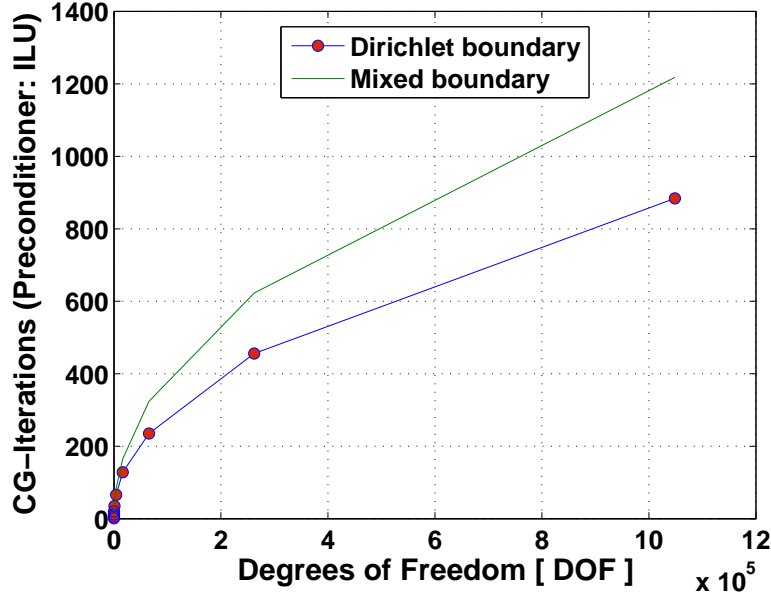
28

Fig. 19. Example (4.4): Number of CG iterations required vs degrees of freedom for pure Dirichlet and mixed problem. Here $\gamma = 0.1$

dition number of discrete system associated with mixed boundary conditions is about four times the condition number of the system associated with pure Dirichlet boundary condition.

Figure 21 presents the effectiveness of the ILU preconditioner for the Dirichlet problem. Figure 22 presents the effectiveness of the ILU preconditioner for the problem with mixed boundary. In both cases, preconditioning by ILU reduces number of CG iterations significantly.

Figures 1, 2, 3(a), 3(b), 10, 11(a) and 11(b) are made by using the freely available package called "E-PIX" [18]. For solving linear system of equations, we are using the freely available package "GMM" [24].
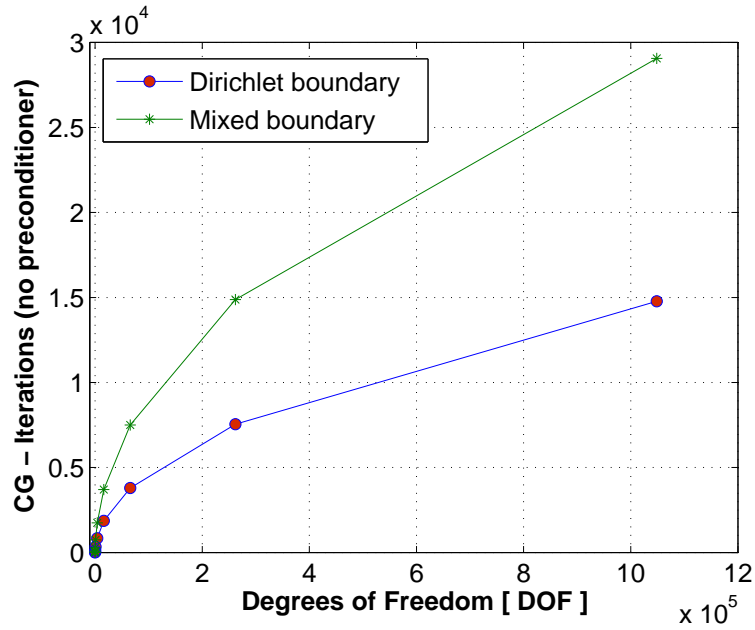
29

Fig. 20. Example (4.4): Number of CG iterations (without any preconditioner) required vs degrees of freedom for pure Dirichlet and mixed problem. Here $\gamma = 0.1$
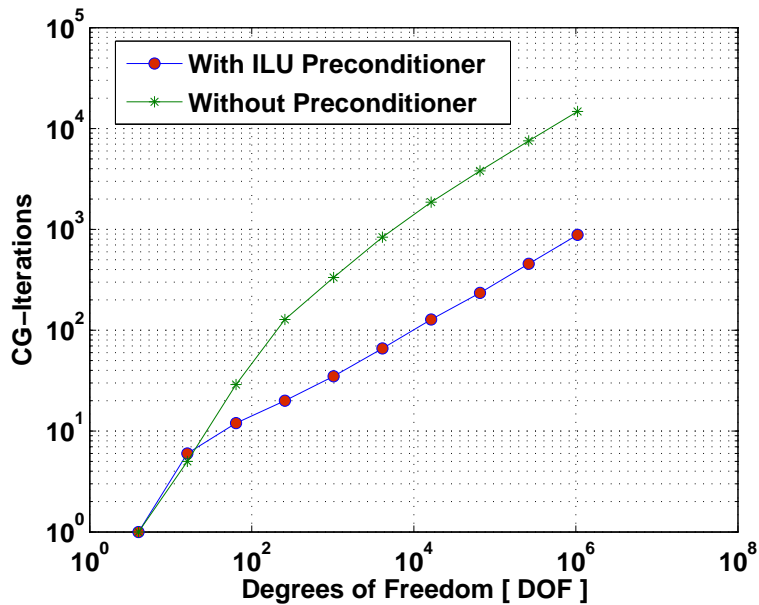

Fig. 21. Example (4.4): Effectivity of the ILU preconditioner for pure Dirichlet problem. Here $\gamma = 0.1$

5 Conclusions

The article has presented convergence analysis of the Two Point Flux Approximation method for single phase flow in a variety of porous mediums such as
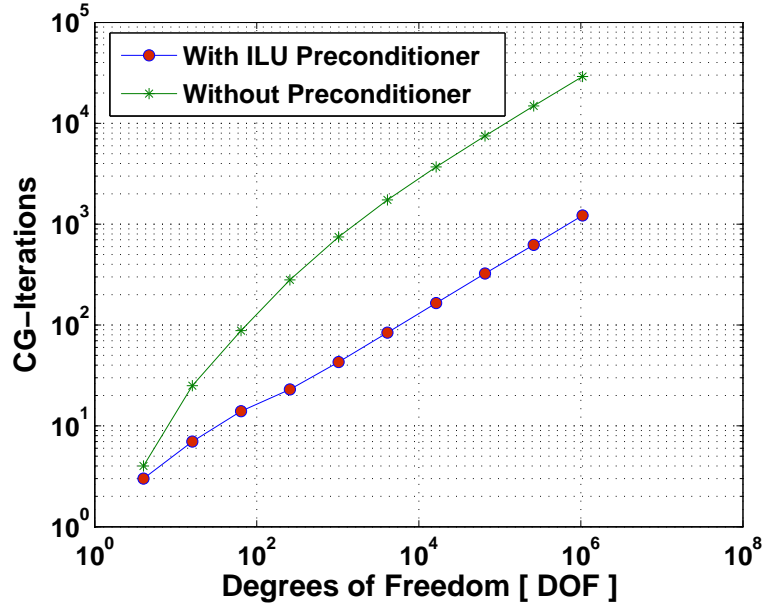
Fig. 22. Example (4.4): Effectivity of the ILU preconditioner for mixed problem. Here $\gamma = 0.1$

isotropic, anisotropic, heterogenous, etc. We have analysed effect of the boundary conditions on the conditioning of the discrete systems and performance of the Conjugate Gradient solver. We also presented the effectiveness of the ILU preconditioner for Dirichlet and mixed boundary conditions.

For problems with regularity $\mathbf{H}^{1+\gamma}$, we are roughly observing the following convergence behaviour

$$\|\mathbf{p} - \mathbf{p}_h\|_{L_2} \approx C\,h^{-2\gamma}\ , \quad \|\mathbf{p} - \mathbf{p}_h\|_{L_\infty} \approx C\,h^{-\gamma}\quad .$$

It was observed that a high degree of singularity ($\gamma \in [0.1, 0.2]$) can retard the convergence behaviour of the method or method may require more than 1,000,000 degrees of freedom for attaining an asymptotic convergence rate. Even after introducing more than a million degrees of freedom, the method

does not converge in the point-wise sense for the extreme singularity $\gamma = 0.1$.

References

[1] *Norsk Hydro Research Center.* First Reference Manual. Internal technical description, 2001.

[2] I. Aavatsmark. An introduction to multipoint flux approximations for quadrilateral grids. *Comput. Geosci.*, 6(3-4):405–432, 2002.

[3] K. Aziz and A. Settari. *Petroleum Reservoir Simulation.* Applied Science Publishers, New York, 1979.

[4] H. Cao. Development of Techniques for General Purpose Simulators. *PhD Thesis, Stanford University.*, 2002.

[5] A. Castellini. Flow based grid for reservoir simulation. *Master Thesis, The Stanford University*, 2001.

[6] S. H. Chou, D. Y. Kwak, and K. Y. Kim. Mixed finite volume methods on nonstaggered quadrilateral grids for elliptic problems. *Math. Comp.*, 72(242):525–539 (electronic), 2003.

[7] Eclipse. Eclipse 100 Technical Description, Schlumberger Geoquest. *Report*, 1997.

[8] M. G. Edwards, R. Agut, and K. Aziz. Quasi K-orthogonal streamline grids: gridding and discretization. In *SPE 49072. Proceedings, SPE Annual Technical Conference and Exhibition, New Orleans, Louisiana, September 27-30*, 1998.

[9] G. T. Eigestad. Reservoir simulation on heterogenous and anisotropic media with imposed flux continuity conditions for general geometries, and the inclusion of hysteresis in forward modeling. *PhD Thesis, The University of Bergen, Norway*, 2003.

[10] G. T. Eigestad, I. Aavatsmark, and M. Espedal. Symmetry and M-matrix issues for the O-method on an unstructured grid. *Comput. Geosci.*, 6(3-4):381–404, 2002. Locally conservative numerical methods for flow in porous media.

[11] G. T. Eigestad and R. A. Klausen. On the convergence of the multi-point flux approximation O-method: Numerical experiments for discontinuous permeability. *Numerical Methods for Partial Differential Equations*, 21(6):1079–1098, 2005.

[12] R. E. Ewing, R. D. Lazarov, and P. S. Vassilevski. Local refinement techniques for elliptic problems on cell-centered grids. I. Error analysis. *Math. Comp.*, 56(194):437–461, 1991.

[13] R. E. Ewing, R. D. Lazarov, and P. S. Vassilevski. Local refinement techniques for elliptic problems on cell-centered grids. III. Algebraic multilevel BEPS preconditioners. *Numer. Math.*, 59(5):431–452, 1991.

[14] R. E. Ewing, R. D. Lazarov, and P. S. Vassilevski. Local refinement techniques for elliptic problems on cell-centered grids. II. Optimal order two-grid iterative methods. *Numer. Linear Algebra Appl.*, 1(4):337–368, 1994.

[15] P. A. Forsyth Jr. and P. H. Sammon. Quadratic convergence for cell-centered grids. *Appl. Numer. Math.*, 4(5):377–394, 1988.

[16] I. Garrido, G. E. Fladmark, and M. Espedal. An improved numerical simulator for multiphase flow in porous media. *Internat. J. Numer. Methods Fluids*, 44(4):447–461, 2004.

[17] I. Garrido, E. Øian, M. Chaib, G. E. Fladmark, and M. S. Espedal. Implicit treatment of compositional flow. *Comput. Geosci.*, 8(1):1–19, 2004.

[18] A. D. Hwang. ePiX: A free utility for creating mathematically accurate LaTex figures. Available at "http://mathcs.holycross.edu/∼ahwang/current/epix.html", 2005.

[19] S. K. Khattri. Analysing an Adaptive Finite Volume for Flow in Highly Heterogenous Porous Media. *Submitted in the Journal of Transport in Porous Media*, 2005.

[20] S. K. Khattri. Numerical tools for multi-component, multi-phase, reactive transport in porous medium. *PhD Thesis, The University of Bergen, Norway*, 2005.

[21] S. H. Lee, H. Tchelepski, and L. F. De Chant. Implementation of a flux continuous finite difference method for stratigraphic, hexahedron grids. In *Proceedings of the SPE Reservoir Simulation Symposium (Houston, Tex.,)*, 1999.

[22] J. M. Nordbotten and G. T. Eigestad. Discretization on quadrilateral grids with improved monotonicity properties. *J. Comput. Phys.*, 203(2):744–760, 2005.

[23] K. Pruess, J. Garcia, T. Kovscek, C. Oldenburg, J. Rutqvist, C. Steefel, and T. Xu. Intercomparison of Numerical Simulation Codes for Geologic Disposal

of CO_2. *LBNL-51813*, December, 2002.

[24] Y. Renard and J. Pommier. GMM^{++} a Generic Template Matrix C^{++} Library. Available at "http://www-gmm.insa-toulouse.fr/getfem/gmm_intro", 2005.

[25] B. Riviere. Discontinuous Galerkin Finite Element Methods for Solving the Miscible Displacement Problem in Porous Media. *PhD Thesis, The University of Texas at Austin*, 2000.

[26] B. Riviere, M.F. Wheeler, and K. Banas. Part II. Discontinuous Galerkin Method Applied to Single Phase Flow in Porous Media. *Computational Geoscience*, 4:337–341, 2000.

[27] L. Saas, I. Faille, F. Nataf, and F. Willien. Finite Volume Methods for Domain Decomposition on Nonmatching Grids with Arbitrary Interface Conditions. *SIAM Journal on Numerical Analysis*, 43(2):860–890, 2005.

[28] G. Strang and G. J. Fix. An analysis of the finite element method. *Wiley New York*, 1, 1973.

[29] E. Süli. Convergence of finite volume schemes for Poisson's equation on nonuniform meshes. *SIAM J. Numer. Anal.*, 28(5):1419–1430, 1991.

[30] H. A. van der Vorst. *Iterative Krylov Methods for Large Linear Systems.* Cambridge monographs on applied and computational mathematics. Cambridge University Press, New York, 2003.

[31] A. Weiser and M. F. Wheeler. On convergence of block-centered finite differences for elliptic-problems. *SIAM J. Numer. Anal.*, 25(2):351–375, 1988.

[32] J. A. Wheeler, M. F. Wheeler, and I. Yotov. Enhanced velocity mixed finite element methods for flow in multiblock domains. *Comput. Geosci.*, 6(3-4):315–332, 2002. Locally conservative numerical methods for flow in porous media.

[33] X. H. Wu and R. R. Parashkevov. Effect of grid deviation on flow solutions. *SPE 92868*, 2005.